Band transport model for discotic liquid crystals

L. J. Lever,[1,*] R. W. Kelsall,[2] and R. J. Bushby[1]
[1]*SOMS Centre, University of Leeds, Leeds LS2 9JT, United Kingdom*
[2]*School of Electronic and Electrical Engineering, University of Leeds, Leeds LS2 9JT, United Kingdom*
(Received 16 February 2005; revised manuscript received 7 April 2005; published 27 July 2005)

A theoretical model is presented for charge transport in discotic liquid crystals in which a charge is delocalized over more than one lattice site. As such, charge transport is via a banded conduction process in a narrow bandwidth system and takes place over coherent lengths of a few molecules. The coherent lengths are disrupted by the geometrical disorder of the system and are treated as being terminated by quantum tunnel barriers. The transmission probabilities at these barriers have been calculated as a function of the charge carrier energy. Phononic interactions are also considered and the charge carrier scattering rates are calculated for intermolecular and intramolecular vibrations. The results of the calculations have been used to develop a Monte Carlo simulation of the charge transport model. Simulated data are presented and used to discuss the nature of the tunnel barriers required to reproduce experimental data. We find that the model successfully reproduces experimental time of flight data including temperature dependence.

DOI: 10.1103/PhysRevB.72.035130 PACS number(s): 73.23.−b

I. INTRODUCTION

Discotic liquid crystals (DLCs) are disk shaped molecules with rigid aromatic cores and flexible alkyl side chains. They self-organize into structures that exhibit columnar stacking order and liquidlike dynamics. DLCs that are free from impurities are good insulators and a charge must be injected before electronic conduction can occur.[1] The carrier mobilities are highly anisotropic and the mobility along the column is $\sim 10^3$ times greater than that perpendicular to the columns.[2] In most cases, charge transport is via holes, and mobilities can be measured using time of flight (TOF) techniques. In a TOF experiment, the DLC is sandwiched between two transparent electrodes and a charge is injected at one electrode via a short pulse of laser light. Charge then drifts to the counter electrode under the influence of the applied field, as illustrated in Fig. 1. The time taken for the sheet of charge to reach the cathode (i.e., the TOF) is measured as the duration of the photocurrent. This may be used to calculate a mobility (assuming that the carrier velocity is proportional to the field) using the equation

$$\mu = \frac{d^2}{V\tau}, \tag{1}$$

where d is the electrode separation, V is the applied potential, and τ the duration of the photocurrent.

Crystalline molecular semiconductors, such as pentacene, exhibit charge carrier mobilities as high as 400 $cm^2/V\,s$ (at low temperatures) and the mechanism for charge transport is widely accepted to be band transport.[3] Amorphous molecular semiconductors, however, show mobilities of 10^{-3} $cm^2/V\,s$ or less and charge transport is widely accepted to be via a molecule-molecule hopping process. Charge carrier mobilities in DLCs range from 2.5×10^{-6} to 0.07 $cm^2/V\,s$ (Ref. 1) and span the gap, both in terms of mobility and ordering, between single crystal and amorphous organic materials.

In DLCs, the question of whether charge transport is banded or hopping depends on the nature of the polaron formation. The presence of an excess charge distorts the surrounding medium, giving rise to the formation of a polaron. Depending on the strength of the coupling between the excess charge and the phonons, large (weak coupling) or small (strong coupling) polarons are formed.[4] If the electronic motion is so fast that it passes a lattice site in a time scale smaller than the time scale of molecular vibrations, then the lattice does not have time to relax to the new distorted geometry while the excess charge remains on that lattice site and the polaron formation can be regarded as a perturbation to the band structure.[5] In this case, a lattice distortion (i.e., a large polaron) is dragged along with the charge causing an increase in effective mass and narrowing of the bandwidth.[4,6] If the electronic motion is slower than the time scale of molecular vibrations, then the lattice does have time to relax to the new distorted geometry and this can act to trap the charge in a localized lattice distortion, or small polaron, and transport is by phonon-assisted hopping between lattice sites.[5]

Hopping is a random-walk process and the Miller-Abrahams formulation shows that the high mobilities found in materials such as hexakis-(hexylthio)triphenylene (HTT6) require hopping rates in excess of 10^{12} Hz. Since DLCs contain imperfections,[7] the actual required hopping rate will probably be much larger than this. Furthermore, phonon-assisted hopping leads to a positive temperature-mobility correlation. However, in higher mobility DLCs, such as HTT6, a weak negative temperature-mobility correlation is

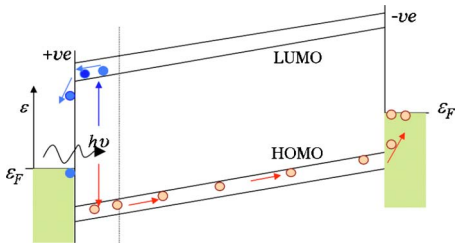

FIG. 1. (Color online) Band diagram illustrating the TOF charge transport process.

 ©2005 The American Physical Society

observed.[8] Even hexakis(n-hexyloxy)triphenylene (HAT6) ($\mu=3\times10^{-4}$ cm^2/V s) shows a weak, almost temperature-independent carrier mobility.[9] Such a temperature dependence of the mobility is easier to understand if the charge transport is via a coherent banding mechanism.

A band transport model is described and its results presented for parameters appropriate to HTT6, which forms a helical phase with rotational ordering between adjacent molecules and exhibits a mobility of 0.07 cm^2/V s (Ref. 8). The description is general, though, and could be extended to any of the higher mobility DLC systems. A band transport model with crystalline imperfections has been developed,[10] and in this paper, the authors aim to set out the theoretical methodology to describe that model fully.

II. MODEL DESCRIPTION

The band was formed according to the tight-binding approach. A single molecular state was considered and a linear combination of these molecular orbitals used to create a band structure. This yields a dispersion relation of the form:

$$\varepsilon(k) = \varepsilon_b(1 - \cos ka), \tag{2}$$

where a is the lattice constant; ε_b is half the bandwidth; which, from the tight-binding Hamiltonian used, is twice the charge transfer integral; and k is the wave vector. The lattice constant for the DLC system is taken to be the core-core repeat distance, which has been determined, from x-ray-scattering experiments, to be 3.5 Å for triphenylenes.[11] The calculations that give the above dispersion relation assume an infinite chain of molecules. A fundamental feature of the model, as described below, is the presence of breaks in the linear molecular chains. If the breaks are closely spaced then the assumption of a periodic linear chain would not be valid. However, our simulation results show that the experimental data are best fitted when the distance between complete breaks in the chain is more than ~200 Å. This corresponds to ~60 molecules, which, in the tight-binding framework, give a set of energy states that are separated by much less than k_BT, hence it can be considered as a continuous band.

There are two types of imperfections to be included in the model. These are displacements in the plane of the molecules and displacements normal to this plane (see Fig. 2)—let these be labeled Δx and Δz, respectively. These imperfections will cause localized perturbations and breaks in the band structure that the charge carrier must tunnel through. The nature of the imperfections and the tunneling process will be addressed in more detail in Sec. III. Rotational disorder will cause constrictions in the band structure that are similar to those for the Δx imperfections. The resulting transmission probabilities will be of the same order or lower, depending on the angular displacement. As such they are included as part of the Δx tunneling process so that the modeled Δx imperfections consider both the in-plane translational and rotational imperfections. It is not expected that this will lead to any significant error because any tunneling process that has a low transmission probability will not be significant in the charge transport process and the coherence length will now be correct.

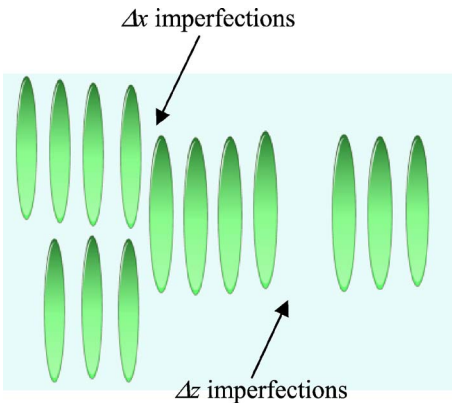

FIG. 2. (Color online) The two disruptions to the geometrical ordering of the DLC considered in the model.

A. The simulation

The simulation technique used is a semiclassical Monte Carlo method. Charge carriers are modeled as point particles each carrying unit electronic charge. The transport simulation is one dimensional and assumes that the field is in the direction parallel to the director of the DLC column, consistent with a homeotropically aligned TOF cell. Carriers are drifted in an electric field F and gain an amount of crystal momentum given by

$$\delta k = \frac{eF\tau}{\hbar}, \tag{3}$$

where e is the electronic charge and τ is a stochastic free flight time, which is determined by phonon-scattering rates (discussed in more detail in Sec. IV). This gain in crystal momentum results in a change of carrier energy in accordance with Eq. (2). The distance traveled by the carrier during a free flight is given by

$$\delta z = \frac{1}{eF}\delta\varepsilon, \tag{4}$$

where $\delta\varepsilon$ is the energy change due to drifting in the field. The carrier is drifted from the charge generation layer at the anode until it has traveled sufficient distance to reach the cathode. The cathode is modeled as a purely ohmic contact, such that when a carrier is incident on it, it is absorbed.

The carriers are assumed not to interact with one another. This follows from considering the photocurrent and the area illuminated by the laser pulse in a TOF experiment: There are roughly 1000 times more columns for charge transport than there are charge carriers. The simulation is repeated many times to generate data for an ensemble of carriers to simulate a current.

III. IMPERFECTIONS

The two imperfections illustrated in Fig. 2 are significant because these changes in structural conformation affect the charge transfer integral, and the bandwidth is dependent on this. For the in-plane dislocation, an axial displacement of half the intercolumnar separation was assumed. This was

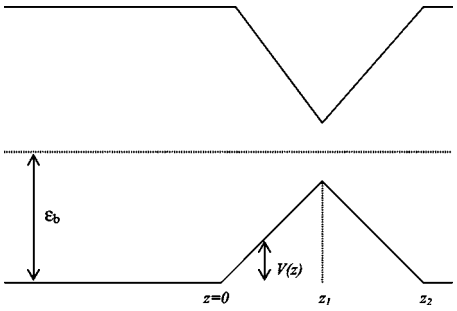

FIG. 3. Energy diagram for band constrictions at Δx imperfections, $z_2 = 10$ Å.

modeled by considering the effect on the valance band and it is expected that the charge transfer integral will decrease, since less of the core area is "in contact," which will cause the bandwidth to decrease proportionally. An in-plane displacement from equilibrium of HTT6 by 10 Å causes the charge transfer integral to change from 0.12 eV to approximately 0.04 eV.[12] Such a dislocation will result in the localized narrowing of the bandwidth and was modeled as a linear constriction as shown in Fig. 3. Various forms of the constriction were considered, including Gaussian and square barriers. A linear constriction was chosen since it approximates a gradual change in bandwidth (which seems more likely than a square constriction) and the energy dependence of transmission probability was very similar to that of a Gaussian one, yet the linear constriction affords an analytical result that can be incorporated into the simulation without the need for lookup tables, which would incur their own errors.

In the region of the constriction, the dispersion relation becomes

$$\varepsilon = V(z) + [\varepsilon_b - V(z)][1 - \cos(ka)], \tag{5}$$

where $V(z) = Az$; $0 < z < z_1$ and $V(z) = -A(z - z_1)$; $z_1 < z < z_2$. Rearranging for k gives

$$k = 1/a \cos^{-1}\left(1 - \frac{[\varepsilon - V(z)]}{[\varepsilon_b - V(z)]}\right) \tag{6}$$

for the regions where $\varepsilon > V(z)$ and, since for $\varepsilon < V(z)$ the result of the above equation will be imaginary, in the tunneling region we have

$$\gamma = 1/a \cosh^{-1}\left(1 - \frac{[\varepsilon - V(z)]}{[\varepsilon_b - V(z)]}\right), \tag{7}$$

which is only valid in the regions $V(z) < \varepsilon < \varepsilon_b$. This means that we can only treat narrowings of the band with this method and not complete breaks.

The Wentzel-Kramers-Brillouin (WKB) formula for tunneling gives a tunneling probability of[13]

$$T_{WKB} = e^{-2\int \gamma(z) dz}, \tag{8}$$

which, for this system, gives a transmission probability of

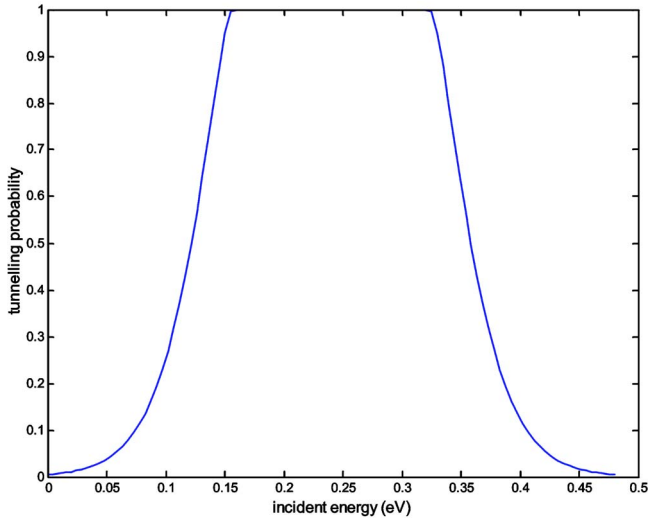

FIG. 4. (Color online) Transmission probability as a function of incident energy for Δx tunnel barriers.

$$T = \exp\left[-\frac{4(\varepsilon_b - \varepsilon)}{aA}\int \frac{\cosh^{-1}(u)}{u^2} du\right], \tag{9}$$

where

$$u = 1 - \frac{\varepsilon - V(z)}{\varepsilon_b - V(z)}. \tag{10}$$

The tunneling probability is shown in Fig. 4 and goes to unity for carriers with greater incident energy than the height of the constriction. A reflection term is expected for this case. However, this will be small and the majority of carriers have incident energies much lower than this and so it has been neglected.

The Δz imperfections illustrated in terms of energy in Fig. 5 cause the overlap integral to disappear completely. This type of imperfection was modeled as an abrupt break in the band using a modified WKB (MWKB) approach.[14] Since there is no band structure in the tunnel barrier region, the dispersion relation within the tunnel-barrier region was taken to be

$$\varepsilon = \frac{\hbar^2 \gamma^2}{2m_e}, \tag{11}$$

where m_e is the free electron mass and γ is the imaginary wave vector. The MWKB approach modifies the standard

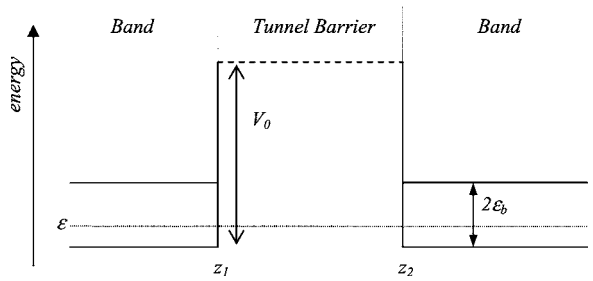

FIG. 5. Energy diagram for Δz tunnel barriers.

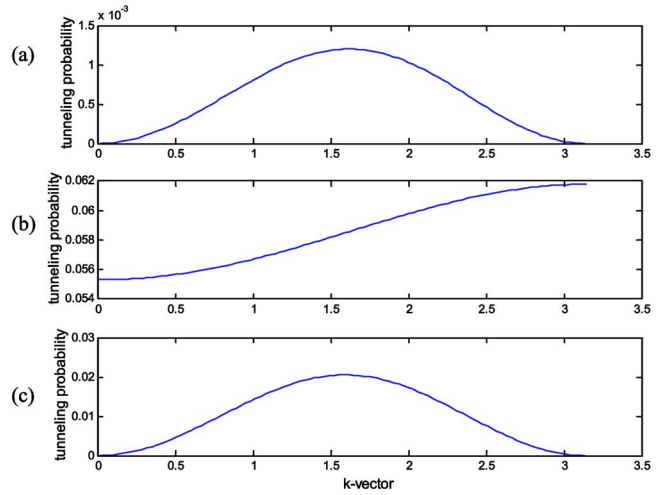

FIG. 6. (Color online) Transmission probabilities for Δz tunnel barriers as a function of incident k vector. (a) Total transmission probability. (b) The WKB term. (c) Group velocity mismatch term.

WKB approach by a group-velocity mismatch term given by

$$T_R = \left(\frac{4\nu_g \nu_g'}{\nu_g^2 + \nu_g'^2} \right)^2, \tag{12}$$

where ν_g is the group velocity in the band and ν_g' is the group velocity in the tunnel region. The mismatch term will be small when the charge carrier energy is low since the group velocity approaches zero for $k \to 0$.

The MWKB transmission probability is shown in Fig. 6; it is dominated by the group-velocity mismatch term T_R and shows transmission probabilities for incident carriers with energies near the center of the band around three orders of magnitude greater than those with energies near the bottom (or top) of the band.

IV. SCATTERING MECHANISMS

Scattering mechanisms included in the model are transverse acoustic phonon-scattering, molecular vibrations causing out-of-plane motion of the triphenylene core and reflective scattering from tunnel barriers. Charged impurity scattering has not been included since the concentration of charged impurities in a well-prepared sample of a liquid crystal is less than one part per billion.[15] A typical TOF cell is $\sim 20\ \mu$m thick giving $\sim 60\,000$ molecules per column, therefore (considering nearest-neighbor columns) the probability of a charged impurity scattering event occurring at all will be $<10^{-3}$ for each carrier. As discussed in Sec. III carrier populations are much smaller than the number of columns, so carrier-carrier interactions may also be neglected.

The transverse phonon-scattering rates were calculated according to the method of Bardeen and Shockley.[16] The transverse vibration about equilibrium positions is assumed to propagate along the columns. The displacement from equilibrium of an individual molecule is given by

$$\delta x = A e^{\pm i(\mathbf{q}\cdot\mathbf{z} - \omega t)}, \tag{13}$$

where A is the amplitude of vibration, $\mathbf{q}$ the wave vector, $\mathbf{z}$ the displacement along the column, x the displacement from equilibrium, ω angular frequency, and t time. If it is assumed that the wavelength of the vibrations is much larger than the lattice spacing, a, then the difference in displacement from their equilibrium positions between adjacent molecules becomes

$$|\delta x(a) - \delta x(0)| = \frac{d}{dz}(\delta x)a, \tag{14}$$

and we have

$$\frac{d}{dz}(\delta x) = \pm i(\mathbf{q}\cdot\mathbf{z}). \tag{15}$$

The acoustic deformation potential constant ε_{ac} describes how strongly the deformation of the lattice interacts with the edge of the valance band

$$\delta\varepsilon = \varepsilon_{ac}\frac{d}{dz}(\delta x). \tag{16}$$

Here $\delta\varepsilon$ is the change in energy of the valance band edge caused by the transverse displacement. A linear fit was applied to data from Ref. 12 to find the change in overlap integral with Δx displacement. The band edge will undergo a shift in energy of twice the overlap integral, and so the gradient of this linear fit multiplied by the lattice constant will give the acoustic deformation potential constant ε_{ac}. For transverse acoustic phonons, this value was found to be 55 meV.

To calculate the scattering rate, a matrix element for the interaction must be found. Following the method of Bardeen and Shockley, this matrix element is given by

$$|H_{k'k}| = \varepsilon_{ac} q A. \tag{17}$$

The quantum analog of the amplitude of molecular vibration, A, is found by considering the transition between the Nth vibrational state to either the $N-1$ or $N+1$ state corresponding to adsorption and emission of a phonon for a harmonic oscillator

$$A = \left| \int \varphi_{N\pm1}^* x \varphi_N d^3 r \right| = \begin{cases} \sqrt{\dfrac{N\hbar}{2M\omega}}, & N \to N-1 \\ \sqrt{\dfrac{(N+1)\hbar}{2M\omega}}, & N \to N+1, \end{cases} \tag{18}$$

where M is the oscillator mass and ω the angular frequency of the vibration and N is the Bose-Einstein factor. Molecular dynamics simulations and fitting to quasi electric neutron scattering (QENS) experiments[12] give a frequency of 5×10^{12} Hz for transverse oscillations.

The Fermi golden rule was used to calculate the scatter rates, giving

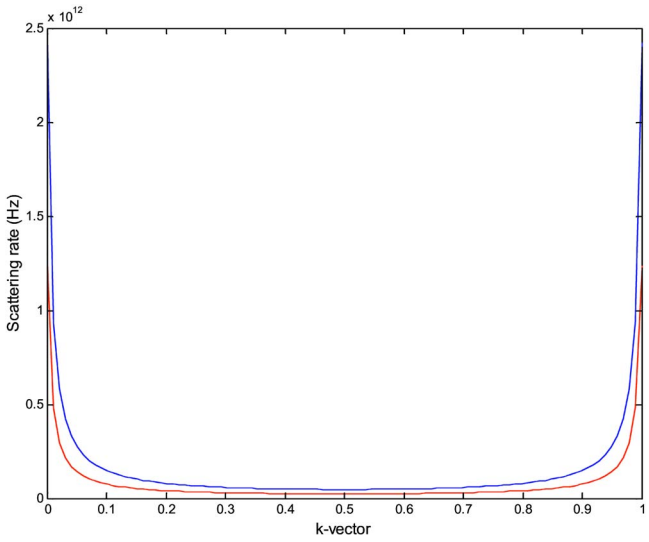

FIG. 7. (Color online) Scattering rates for transverse acoustic phonons as a function of *final state k* vector. Emission rates are shown by the dashed line and absorption by the dotted line.

$$P_{em}(k) = \frac{2\pi}{\hbar}\varepsilon_{ac}^2 q^2 \frac{(N+1)\hbar}{2M\omega}\rho_{k'} \tag{19}$$

for phonon emission and

$$P_{abs}(k) = \frac{2\pi}{\hbar}\varepsilon_{ac}^2 q^2 \frac{N\hbar}{2M\omega}\rho_{k'} \tag{20}$$

for absorption where k is the initial state wave vector and $\rho_{k'}$ is the density of final states given by

$$\rho_{k'} = \frac{L}{\pi}\frac{1}{a\varepsilon_b \sin k'a}, \tag{21}$$

where k' is the final state wave vector. Expressing the scattering rates in terms of final state wave vector yeilds

$$P_{em}(k) = \varepsilon_{ac}^2 \frac{2\pi^2}{a^3}\frac{(N+1)}{\varepsilon_b \rho\omega}\frac{1}{S}\frac{1}{\sin k'a} \tag{22}$$

for emission and

$$P_{abs}(k) = \varepsilon_{ac}^2 \frac{2\pi^2}{a^3}\frac{N}{\varepsilon_b \rho\omega}\frac{1}{S}\frac{1}{\sin k'a} \tag{23}$$

for absorption, where S is the cross-sectional area of the molecular cores. The phonon-dispersion relation has been approximated to a linear relationship and q replaced with π/a. The scattering rates are shown as a function of the final state wave vector in Fig. 7. The scattering rates become much higher as carriers are scattered to the edge of the band as the density of states is larger here.

The scattering rates for the C-H bond flexing may be calculated in a similar way. The matrix element for a scattering process can be expressed as

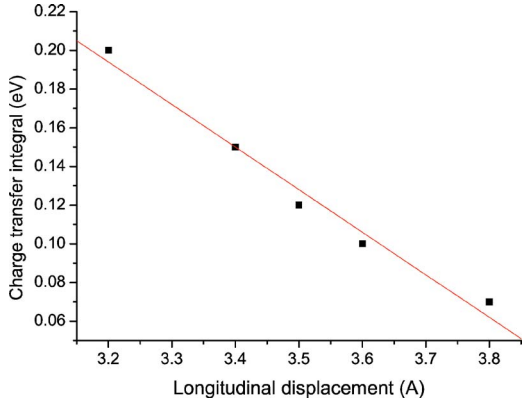

FIG. 8. (Color online) Variation of charge-transfer integral with longitudinal displacement.

$$|H_{kk'}| = \int \psi_{k'}^* V(r)\psi_k d^3 r. \tag{24}$$

The potential $V(r)$ describes the magnitude of the change in valence band-edge energy and, since we are considering a longitudinal vibration, this will be the product of twice the gradient of the plot of charge transfer integral with longitudinal displacement, shown in Fig. 8. Let this gradient be ε_{CH} (this is not the same as the constant ε_{ac} found in the previous argument since we are dealing with molecular vibration and not an acoustic phonon). The amplitude of the vibration will also be much smaller than for an acoustic phonon because a C-H bond flexing mode is under consideration. The amplitude of vibration for a hydrogen atom is ~1 Å; given the ratio of the masses of the six hydrogen atoms around the core to the mass of the remainder of the molecule, this gives an amplitude for the vibration for the molecule of ~0.007 Å. This is comparatively small, but from the gradient of Fig. 8 it follows that a displacement of 0.007 Å will perturb the valance band edge by 3.2 meV, which is 1.3% of the bandwidth.

Expressing ψ as

$$\psi = \frac{1}{\sqrt{V}}u_k(r)e^{i(k.r-\omega t)}, \tag{25}$$

where V is volume and u_k is a Bloch function, which cancels and allows the matrix element to be written as

$$|H_{kk'}| = \frac{1}{V}\varepsilon_{CH} A \int e^{i(k-k'-q)}d^3 r = \varepsilon_{CH} A\,\delta(k-k'q), \tag{26}$$

where q is the effective crystal momentum of the lattice vibration.

Assuming a harmonic oscillator for the molecular vibrations and treating a scattering event is a transition from the Nth to the $N\pm1$th vibrational state for quantized molecular vibrations A may be expressed as in Eq. (18). Appling the Fermi golden rule and using the density of final states in Eq. (21) gives scattering rates of

$$P_{em}(k') = \varepsilon_{CH}^2 \frac{(N+1)}{a\varepsilon_b \rho\omega}\frac{1}{S}\frac{1}{\sin k'a} \tag{27}$$

for emission and

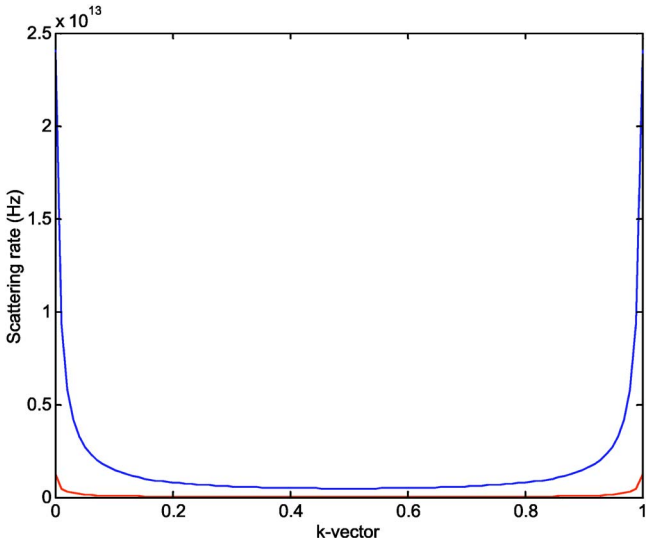

FIG. 9. (Color online) Scattering rates for the C-H bond flexing phonon as a function of *final state k* vector. Emission rates are shown by the dashed line and absorption by the dotted line.

$$P_{abs}(k') = \varepsilon_{CH}^2 \frac{N}{a\varepsilon_b \rho\omega} \frac{1}{S} \frac{1}{\sin k'a} \tag{28}$$

for absorption. The Bose-Einstein factor has been calculated here using the frequency of 2.22×10^{13} Hz corresponding to the ir absorption frequency for triphenylene C-H bond flexing.

The scattering rates for the C-H bond flexing mode are shown in Fig. 9. They display a greater difference between emission and absorption rates than for the transverse acoustic phonon. This is because the energy of the vibrational state is greater, hence the Bose-Einstein factor is smaller and the ratio $(N+1)/N$ is larger. The transverse acoustic phonon scattering rates are $\sim10^{11}$ Hz and for the C-H flexing mode $\sim10^{11}$ Hz for absorption and $\sim10^{12}$ Hz for emission.

Carriers are also scattered by tunnel barriers. If a carrier tunnels through a barrier its wave vector remains unchanged. When a carrier is reflected from a tunnel barrier its wave vector is reversed. Therefore, barrier scattering is an elastic process.

V. TEMPERATURE DEPENDENCE OF COHERENCE LENGTH

The Δz barriers shown in Fig. 2 will be dynamic since the forces on the molecules will be unbalanced. In other words, the Δz barriers are the result of longitudinal molecular vibrations. The amplitude of the motion has been measured using QENS techniques[17] and found to be ~1.2 Å. This motion is so large as to completely destroy the charge transfer integral as the molecules move apart, and hence it cannot be treated as a perturbation to the band structure as is the case for transverse molecular vibrations. Being the result of a molecular motion, the population of these imperfections is expected to show a temperature dependence and follow Bose-Einstein statistics.

Let the total coherence length l_c be due to two coherence lengths due to Δx and Δz imperfections

$$\frac{1}{l_c} = \frac{1}{l_c^{\Delta x}} + \frac{1}{l_c^{\Delta z}}. \tag{29}$$

As temperature is increased, $l_c^{\Delta z}$ will decrease according to

$$l_c^{\Delta z}(T) = l_c^{\Delta z}(T_0)\frac{N(T_0)}{N(T)}, \tag{30}$$

where T_0 is some reference temperature for which $l_c^{\Delta z}$ can be defined and N is the Bose-Einstein factor for the oscillations. The frequency of these oscillations is 1.4×10^{11} Hz.[17] These molecular vibrations are slow compared to the motion of the charge carriers. Consequently the longitudinal vibrations can be considered as static imperfections of the ordering of the DLC column.

The Δx imperfections are also expected to show a temperature dependence, however the form of it is not known. They are a result of the liquidlike dynamics of the DLC and not a vibration; hence, they will probably not follow Bose-Einstein statistics as the Δz imperfections do (although their population will doubtless increase with temperature). Furthermore, since the Δz imperfections have much lower transmission probabilities, they have a greater effect of the mobility (they have more "stopping power") and so the population of the Δx barriers will be less significant in any case.

Δz imperfections will also exist as the result of the liquidlike dynamics of the system and as such may not follow Bose-Einstein statistics perfectly. However, it is reasonable to assume that the temperature dependence of $l_c^{\Delta z}$ will follow a relationship of a similar form to that given by the Bose-Einstein statistics (i.e., disorder will increase with temperature).

VI. RESULTS

The simulation was designed to generate TOF data. The principal result was the time taken for carriers to drift from one electrode to the other and from this the mobility was calculated. Other simulated data include phonon-scattering statistics, energy and k space distributions, real-space distributions, and tunneling probabilities. The simulation was parametrized for electric field, bandwidth, phonon-scattering rates and energies, temperature effects due to phonons, coherence length, overall temperature dependence (i.e., that due to phonon interaction and due to coherence length reduction), and tunnel barrier dimensions. The effects of varying these parameters will be addressed one by one in this section. First however, it is instructive to look at energy and k-space distributions as well as real-space distributions.

Figure 10(a) shows the charge carrier energy distribution. It is centerd around the bottom of the energy spectrum (which, for holes means they are at the top of the valance band, as expected). k_BT is 31 meV at this temperature (358 K) and so carriers are expected to have about half this energy (as there is one degree of freedom) plus that gained from the field. The mean carrier energy is around 20 meV. Figure

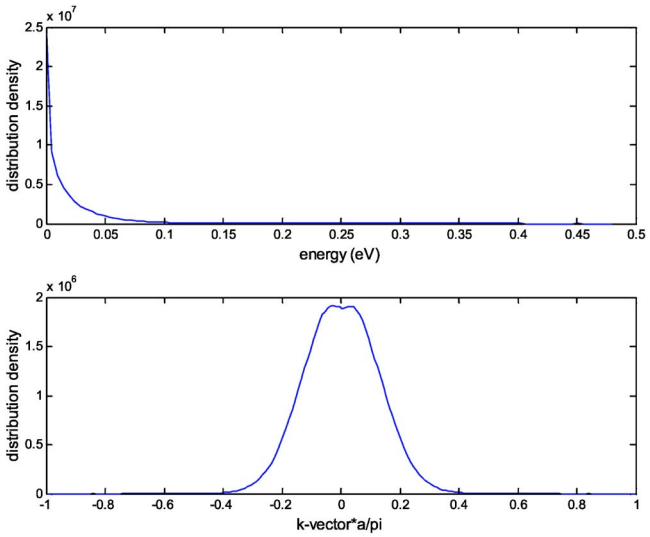

FIG. 10. (Color online) Energy and k-space distributions. The units of distribution density are arbitrary and are merely a count of the number of times the particle occupies that state.

10(b) reveals that the k-space distribution is roughly symmetrical; this implies that carrier group velocities are much greater than the drift velocity contributing to the TOF. The distribution extends to slightly higher positive k values than negative ones, corresponding to the net drift of charge carriers.

Position estimators (Fig. 11) show that carriers tend to "bunch up" behind the more severe Δz barriers, eventually tunneling through them to continue down the column. (It is misleading to consider an ensemble of carriers bunching up behind a single barrier, as it is the amount of time a single carrier spends in a given location that is increasing. However, this provides a more intuitive interpretation of the data.)

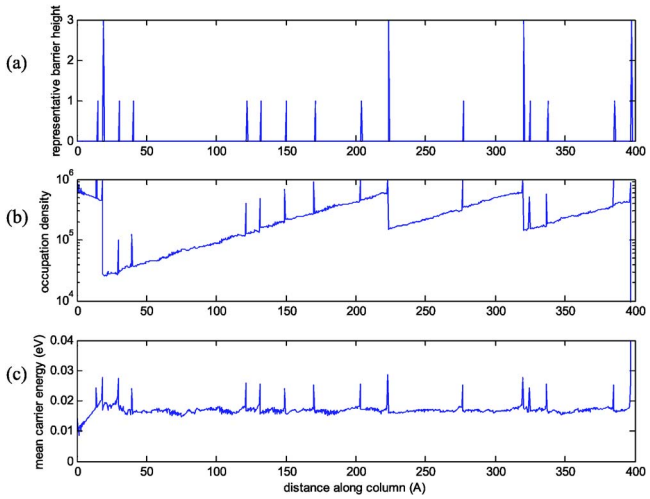

FIG. 11. (Color online) (a) Position of barriers (this is an arbitrary scale and for illustrative purposes only). Δx barriers are shown at a height of 1 and Δz barriers a height of 3. The length of DLC was split up into 2000 "bins." (b) The number of counts of carriers occupying a given bin to give position density estimators. (c) Mean carrier energy as a function of position.

Δz transmission probabilities are $\sim 10^{-4}$, whereas those for the Δx barriers are $\sim 10^{-2}$, this is reflected in the carrier spatial distributions. Populations are artificially peaked at barriers; this is because, in the simulation, estimator values are sampled at every scattering event and barrier reflections are included as scattering events. The spatial distributions show an exponential rise in occupation density as an Δz barrier is approached.

The mean carrier energy is constant along the column at about 20 meV, as is expected. Values are peaked slightly at the site of the barriers. The reason for this is unclear, although it may result from the fact that more carriers impinge on barrier traveling in the direction of the field, and hence they will pick up energy from the field during their free flight. These carriers will thus have a higher mean energy than carriers that are moving in the direction antiparallel with the field. In any case, the peaking of energies at the barriers is merely an artifact of the method of data sampling used in the simulation.

A. Electric field

Charge carrier mobility is defined as the gradient of the velocity field curve. If the group velocity is proportional to the applied electric field then Eq. (1) holds and the charge carrier mobility is field independent. Figure 12(a) shows the simulated carrier velocity as a function of electric field. This is in good agreement with the experimental data plotted in Fig. 12(b) and confirms that the model provides a field-independent charge carrier mobility with velocity proportional to the applied electric field.

B. Bandwidth

The bandwidth is defined as the difference in energy between the top edge and bottom edge of the valence band. From the tight-binding Hamiltonian used here, this value is four times the charge-transfer integral. This has been calculated to be 0.12 eV (Ref. 12) giving a bandwidth of 0.48 eV.

Calculations of the polaronic bandwidth narrowing have been carried out for oligoacenes,[6] which show that the highest occupied molecular orbital (HOMO) bandwidth of naphthalene narrows by about 90% as temperature increased from absolute zero to room temperature. The nature of the carrier-lattice interaction is likely to be significantly different in DLCs to that of an organic crystal phase solid such as naphthalene and, as such, polaronic bandwidth narrowing has not been taken into consideration in the development of this model. However, it is clear that reducing the bandwidth will reduce the mobility, since group velocity is related to bandwidth. Figure 13 shows how the mobility changes as the bandwidth is reduced. It was generated using a Δz tunnel barrier width of 1.7 Å instead of 2.7 Å, as reducing the bandwidth to very small values without increasing the transmission probabilities will result in very low mobilities and excessively long simulation run times.

The mobility dependence on bandwidth follows a power law for small bandwidths (<100 meV); as bandwidth is increased the dependence becomes less strong. This is because transmission probabilities are higher for carriers with ener-

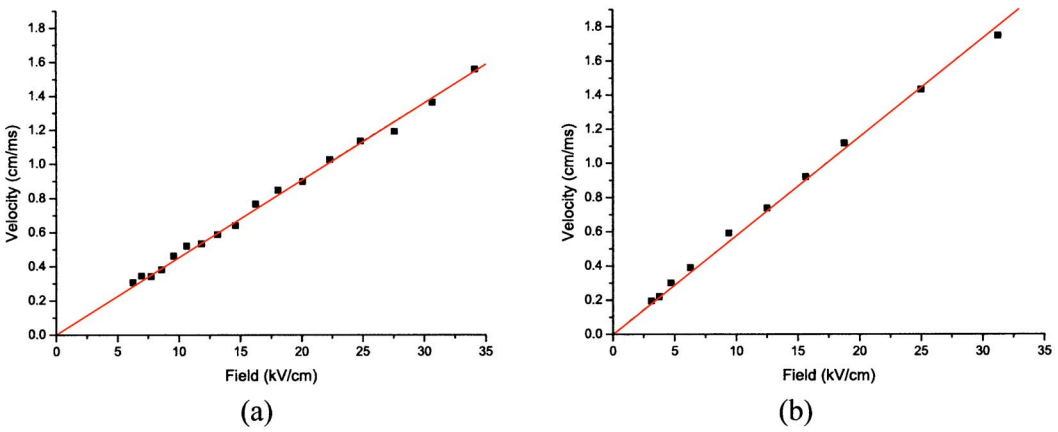

FIG. 12. (Color online) Velocity-field curves at 358 K. (a) Simulated data, electrode separation =2 μm. (b) Experimental data (Ref. 20), electrode separation =23 μm. Although the electrode separations are different (to save CPU time), the carrier velocity is a bulk property and does not show a dependence on the electrode separation.

gies at the middle of the band. For small bandwidths, where k_BT is of the order of half the bandwidth, carriers have energies near the middle of the band and increasing the bandwidth greatly increases mobility. Once the bandwidth has increased so much that population densities at energies near the middle of the band becomes very low, increasing it further reduces the transmission probability and the mobility dependence upon bandwidth becomes weaker.

C. Temperature effects due to carrier-phonon interactions

From Eqs. (22), (23), (26), and (27) it can be seen that there is a temperature dependence of the scattering rate. Furthermore, the ratio of the probabilities of phonon absorption, P_{abs}, and emission, P_{em}, are given by the Bose-Einstein statistics

$$P_{em} = P_{abs}\left(\frac{N+1}{N}\right), \tag{31}$$

where N is the Bose-Einstein factor. The temperature dependence due to carrier-phonon interactions shows a positive correlation between mobility and temperature.

The temperature dependence of the mobility is approximately linear (see Fig. 14), and over the range of the helical phase of HTT6 (345 K to 365 K) varies by ~3%. This constitutes a temperature dependence (due to phonons) that is very weak, almost too weak to be measured by experiment.

The origin of the positive correlation is an increase in the mean carrier energy. Scattering rates increase with increasing temperature and the ratio between the emission and absorption rates decreases. The emission rates are higher than the absorption rates and increasing the temperature increases the mean carrier energy because the ratio between the emission and absorption rates is reduced. Since the tunneling processes are energy dependent, this results in an increase of transmission probability and hence the mobility.

D. Phonon scattering rates and energies

As described in Sec. IV, two phonon energies were used in the simulation [transverse acoustic (20 meV) and C–H bond flexing (92 meV)]. The absorption scattering rates were varied independently for both transverse acoustic and C–H bond flexing processes and the resulting mobilities plotted in Fig. 15 over a temperature of 300–500 K.

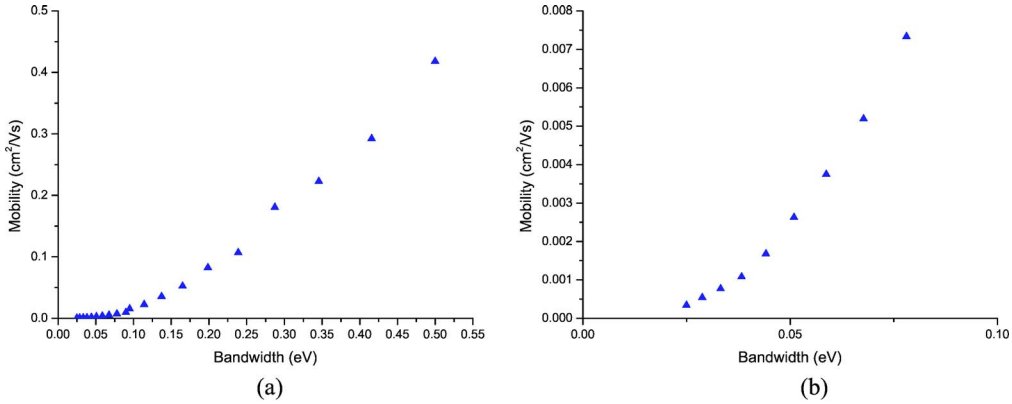

FIG. 13. (Color online) Dependence of the charge carrier mobility on the electronic bandwidth; (b) is a close-up of the small bandwidths shown in (a).

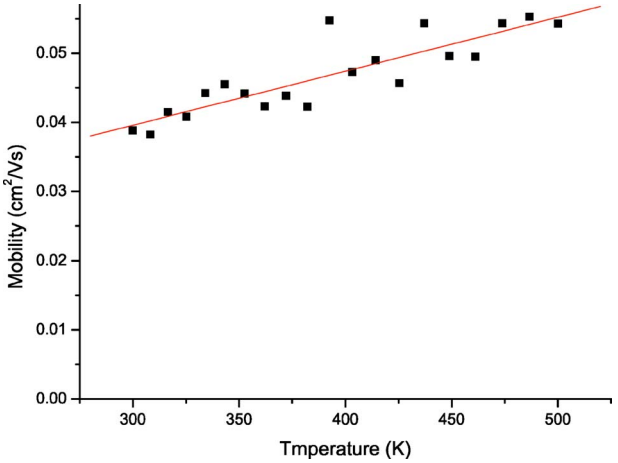

FIG. 14. (Color online) The temperature dependence of mobility due to carrier-phonon interactions shows a weak positive correlation.

The mobility is more strongly dependent on the scattering rate of the 92 meV C-H bond flexing phonon than on the 20 meV transverse acoustic phonon. This suggests that the 92 meV phonon is the most important one for charge transport. The reason for this is that absorption of the 92 meV phonon increases the carrier energy to a level much higher than k_BT. A charge carrier with such an energy will have a higher transmission probability upon encountering a barrier than one at or around k_BT. Therefore, increasing the scattering rate for this phonon actually increases the charge carrier mobility.

E. Temperature effects (including coherence length)

The coherence length is defined as the mean distance along the column over which the highly ordered state persists uninterrupted by imperfections. This has been probed by low angle x-ray experiments and shown to be around 12 nearest neighbors, corresponding to 42 Å.[18] The mobility was found to vary approximately proportionally to the coherence length (for a fixed ratio between the two types of imperfection).

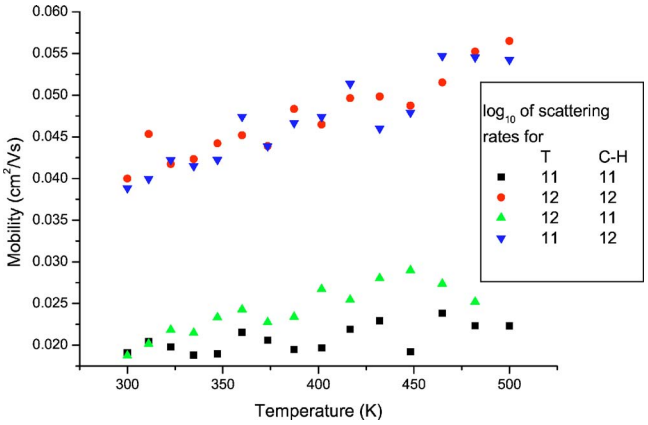

FIG. 15. (Color online) Scattering rates for transverse acoustic (T) and C-H bond flexing (C-H) varied independently.

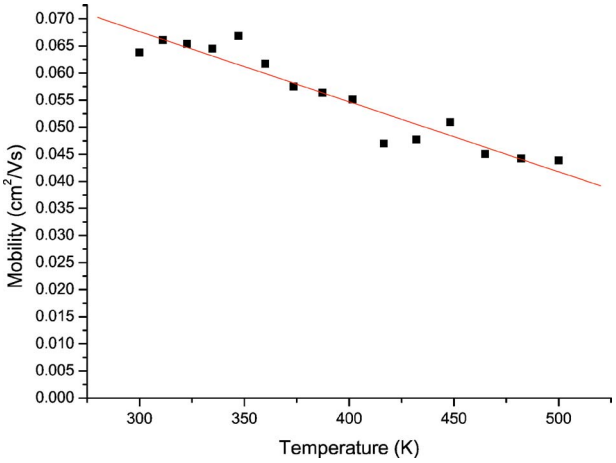

FIG. 16. (Color online) Temperature dependence of system including coherence length-temperature relationship.

The correlation between coherence length and mobility is much stronger than the mobility-temperature correlation due to phonon scattering. Inclusion of the coherence length-temperature relationship discussed in Sec. V results in the carrier mobility as a function of temperature shown in Fig. 16. It shows that the overall temperature dependence is still weak, but shows a negative correlation between temperature and mobility. This negative correlation demonstrates that the temperature effects of coherence length are stronger than the temperature effects due to phonons. Furthermore, it is in agreement with Ref. 8, which shows a weak negative correlation between temperature and mobility, over the range of temperatures at which the helical phase exists.

F. Tunnel barrier dimensions

Of the two tunneling processes described in Sec. III, the Δz (complete break) tunnel barriers are the most significant since the transmission probability for these is considerably lower then for the partial breaks. The transmission probabilities for these barriers are strongly dependent on the barrier width and on the barrier height (see Fig. 17). Both parameters can be varied in order to obtain the desired transmission probabilities. The barrier width was assumed to be 2.7 Å in order to model the longitudinal vibrations that could not be modeled as carrier-phonon interactions. The barrier height was varied in order to fit the experiment. The theoretical limit for the barrier height will be the work function of the DLC, which is approximately 6 eV (Ref. 19).

The dependence of the mobility on the tunnel barrier dimensions is strong. Furthermore, the dependence of the mobility on barrier width is exponential. The transmission probability also depends exponentially on the barrier width; therefore, the mobility is proportional to the transmission probability. This and the fact that the mobility varies proportionally with coherence length imply that the Δz tunnel barriers are the limiting factor for charge transport.

In this model, the slow longitudinal intermolecular motions are modeled as tunnel barriers and are clearly decoupled from the electronic motion and so will not contribute to

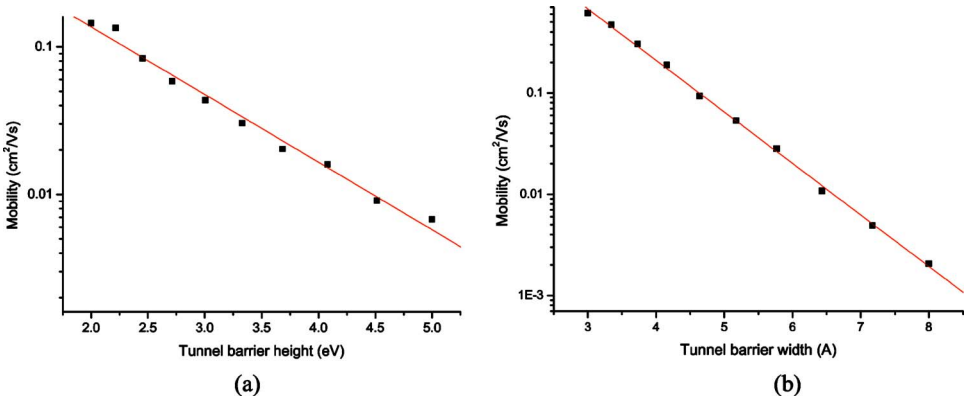

FIG. 17. (Color online) Mobility as a function of (a) Δz barrier height and (b) width.

significant polaronic narrowing of the bandwidth. The faster transverse intermolecular motions are on a time scale of 2×10^{-13} sec, which is also slow compared to electronic motion. The intramolecular motions are on time scales of $\sim 10^{-14}$ sec and this is fast enough to couple to the electronic motion and some degree of polaronic bandwidth narrowing is expected.

The form of the polaronic bandwidth narrowing (i.e., increasing of the effective mass of the carriers) is not known, however, and no reasonable estimate is available. As such it has not been included in the model; however, it is possible to speculate on the implications for the model as bandwidth is reduced. The effect of increasing further the effective mass of the carriers will reduce the group velocity and will also reduce the transmission probabilities at the boundaries between coherent domains, since this is dependent on the group velocity mismatch. In order to fit to experimental data, it will require that the dimensions of the tunnel barriers be reduced. In any case, this detail does not alter the essence of the model: that being one of charge carriers localized over a coherent domain of a few molecules, remaining for a certain characteristic time, which depends mainly on the bandwidth of the carriers and the transmission probabilities at the boundaries.

VII. CONCLUSIONS

A theoretical model has been presented for charge transport in DLCs in which charge is localized over more than one single molecule. DLCs that are well ordered show considerable banding overlap between adjacent molecules and this may persist over a domain that is tens of molecules long before being disrupted by geometrical disorder. Therefore, it is possible for bandlike conduction to take place over a domain of many sites.

Results from the model show that, for HTT6, the experimentally observed mobilities of $\sim 0.06\ \mathrm{cm}^2/\mathrm{V\,s}$ can be reproduced. Such values have previously been associated with models based on hopping transport in a disordered system. In the present model, the mobility is limited by the transmission probabilities at the tunnel barriers, which appear at the interfaces between each well-ordered domain. The model shows that the DLC must contain barriers at which the charge transfer integral between adjacent molecules vanishes. These can either be 'static' defects (which will heal after a certain characteristic reorganization time) or dynamic defects due to molecular vibrations. Either way they represent a carrier-lattice interaction that reduces mobility.

The deformation potential approach to carrier-lattice interactions is not appropriate to describe the large amplitude motion in the DLC system as it cannot be considered a perturbation to the band structure. The tunnel barriers present a method of modeling a banded transport system that interacts strongly with the lattice and exhibits some degree of charge carrier localization. Weakly interacting vibrational modes are modeled using the deformation potential approach. More strongly interacting modes are modeled using the tunnel barrier approach.

The effects of temperature manifest themselves in two ways: through carrier-phonon interactions and by increasing the disorder of the system. The increase of phonon population increases mean carrier energy and hence increases the transmission probabilities at the barriers. The length of the coherent domains decreases with temperature and this reduces the mobility. The mobility-temperature correlation is therefore a trade-off between the increase of transmission probabilities and the decrease of coherent domain size. Irrespective of the precise balance of these two processes, the overall temperature dependence remains weak, which is consistent with experimental findings and in contrast with the trends predicted by simple hopping theories.

ACKNOWLEDGMENTS

The authors would like to thank Bijan Movaghar for invaluable conversations in the developmental stages of this work. Without his input this work would not have been possible.

*Corresponding author. Email address: leonl@chem.leeds.ac.uk

[1] R. Bushby and O. Lozman, Curr. Opin. Solid State Mater. Sci. **6**, 569 (2003).
[2] N. Boden, R. Bushby, J. Clements, B. Movaghar, K. Donovan, and T. Kreouzis, Phys. Rev. B **52**, 13274 (1995).
[3] N. Karl, Synth. Met. **133-134**, 649 (2003).
[4] G. Mahan, *Many Particle Physics* (Kluwer, Dordrecht, 2000).
[5] K. C. Kao and W. Hwang, *Electrical Transport in Solids with Particular Reference to Organic Semiconductors* (Pergamon Press, New York, 1981).
[6] K. Hannewald, V. Stojanovic, and P. Bobbert, J. Phys.: Condens. Matter **16**, 2023 (2004).
[7] A. Pecchia, O. R. Lozman, B. Movaghar, N. Boden, R. J. Bushby, K. J. Donvan, and T. Kreouzis, Phys. Rev. B **65**, 104204 (2002).
[8] D. Haarer, D. Adam, and P. Schuhmacher, Nature (London) **371**, 141/143 (1994).
[9] N. Boden, R. J. Busby, J. Clements, K. Donovan, B. Movaghar, and T. Kreouzis, Phys. Rev. B **58**, 3063 (1998).
[10] L. Lever, R. Kelsall, and R. Busby (unpublished).
[11] R. Bushby and O. Lozman, Curr. Opin. Colloid Interface Sci. **7**, 343 (2002).
[12] K. Senthilkumar, F. Grozema, F. Bickelhopt, and L. Siebbeles, J. Chem. Phys. **119**, 9809 (2003).
[13] D. K. Ferry, *Quantum Mechanics—An Introduction for Device Physicists and Electrical Engineers* (Institute of Physics Publishing, Bristol, 1995).
[14] L. E. Register, E. Rosenbaum, and K. Yang, Appl. Phys. Lett. **74**, 457 (1999).
[15] A. Sawada, Y. Nakazono, K. Tarumi, and N. S, Mol. Cryst. Liq. Cryst. Sci. Technol., Sect. A **331**, 2317 (1999).
[16] J. Bardeen and W. Schockley, Phys. Rev. **80**, 72 (1950).
[17] L. Siebbeles, F. Mulder, J. Stride, S. Picken, P. Kouwer, M. De Haas, and G. Kearley, J. Am. Chem. Soc. **125**, 3860 (2003).
[18] L. Y. Chiang, C. R. Safinya, N. A. Clark, K. S. Liang, and A. N. Bloch, J. Chem. Soc., Chem. Commun. **11**, 695 (1985).
[19] N. Boden, R. Busby, J. Clements, and B. Movaghar, J. Appl. Phys. **83**, 3207 (1997).
[20] H. Iino and J. Hanna (unpublished).